PAPER

Mathematical modeling of chemotaxis guided amoeboid cell swimming

To cite this article: Qixuan Wang and Hao Wu 2021 Phys. Biol. 18 045001

View the $\underline{\text{article online}}$ for updates and enhancements.



IOP ebooks™

Bringing together innovative digital publishing with leading authors from the global scientific community.

Start exploring the collection-download the first chapter of every title for free.

Physical Biology



RECEIVED 10 January 2021

REVISED 25 March 2021

ACCEPTED FOR PUBLICATION 14 April 2021

PUBLISHED 19 May 2021 PAPER

Mathematical modeling of chemotaxis guided amoeboid cell swimming

Qixuan Wang^{1,2,*} and Hao Wu³

- ¹ Department of Mathematics, University of California, Riverside, CA, United States of America
- Interdisciplinary Center for Quantitative Modeling in Biology, University of California, Riverside, CA, United States of America
- Department of Polymer Science and Engineering, University of Massachusetts, Amherst, MA, United States of America
- * Author to whom any correspondence should be addressed.

E-mail: qixuanw@ucr.edu

Keywords: amoeboid cell swimming, chemotaxis, bacterial rheotaxis, finite volume method, low Reynolds number swimming, reaction—diffusion—convection equation

Supplementary material for this article is available online

Abstract

Cells and microorganisms adopt various strategies to migrate in response to different environmental stimuli. To date, many modeling research has focused on the crawling-based *Dictyostelium discoideum* (Dd) cells migration induced by chemotaxis, yet recent experimental results reveal that even without adhesion or contact to a substrate, Dd cells can still swim to follow chemoattractant signals. In this paper, we develop a modeling framework to investigate the chemotaxis induced amoeboid cell swimming dynamics. A minimal swimming system consists of one deformable Dd amoeboid cell and a dilute suspension of bacteria, and the bacteria produce chemoattractant signals that attract the Dd cell. We use the *mathematical amoeba model* to generate Dd cell deformation and solve the resulting low Reynolds number flows, and use a moving mesh based finite volume method to solve the reaction—diffusion—convection equation. Using the computational model, we show that chemotaxis guides a swimming Dd cell to follow and catch bacteria, while on the other hand, bacterial rheotaxis may help the bacteria to escape from the predator Dd cell.

1. Introduction

Cell migration, an integrated molecular process involving biochemical cascades intercorrelated with external chemical and mechanical stimuli, continues throughout the life span of many organisms [1]. Different microorganisms adopt various propulsion mechanisms and directed locomotion strategies for searching for food/running from predators. For example, individual cells and micro-organisms such as C. reinhardtii and spermatozoa find food by a combination of taxis and kinesis using a flagellated or ciliated mode of swimming [2-5]. Other cell migration processes use the highly motile amoeboid mode, whose underlying molecular mechanisms have been extensively studied [6]. Amoeboid (e.g. Dictyostelium discoideum or leukocytes) cell migration relies on the generation, protrusion, and sometimes even travel of either pseudopodia or blebs [7]. As for strategies for directed locomotion, many flagellated bacteria (e.g. E.

coli, S. marcescens, and V. alginolyticus) and even some eukaryotic organisms such as the green algae C. reinhardtii adopt a run- and-tumble type of motility [8]. During the run stage, the bacterium performs a more or less linear motion, while during the tumble stage it performs a highly erratic motion that produces little translocation but reorients the cell, thereby generating a random direction for the next run [9-11]. On the other hand, amoeboid cells detect extracellular chemical and mechanical signal gradients via membrane receptors, and these trigger signal transduction cascades that produce intracellular signals. Small differences in the extracellular signal are amplified into large end-to-end intracellular differences that control the motile machinery of the cell and thereby determine cell polarization and sites of pseudopod or bleb generation [12–18].

Due to their genetic, biochemical and cell-biolo gical tractability, the social amoebae—*Dictyostelium discoideum* (Dd) have been a microorganism of choice

to study basic processes in morphogenesis, including cell-cell chemical signaling, signal transduction, and cell motility [6, 19-22]. Crawling-based chemotaxisdriven Dd migration, at both individual and collective levels, has been well studied via both models and experiments [23-35]. To date, amoeboid cell migration and taxis are generally studied as the cells crawl on various solid substrates, relying on pseudopods attaching to the substrate. Recently, it was discovered that Dd cells can occasionally detach from the substrate and stay completely free in suspension for a few minutes before they slowly sink; during the free suspension stage, cells continue to form pseudopods that convert to rear-ward moving bumps, thereby propelling the cell through the surrounding fluid in a totally adhesion-free fashion [36]. Also, a mutant of Dd, sadA, which attaches poorly to a substrate, appears nevertheless to migrate normally and does so with an enhanced speed [37]. In the experiments, cells actively swam to a point source of cAMP, compared to no directed motion when the cAMP source is absent [37]. Furthermore, a similar adhesion-independent swimming model involving large-scale shape deformation of the cell body may be adopted by other cells, in particular, traditionally well known crawling cells: for example, human neutrophils swim to a chemoattractant fMLP (formyl-methionylleucyl-phenylalanine) source at a speed similar to that of cells migrating on a glass coverslip under similar conditions [37]. Most recently and equally striking, cytokine can induce Drosophila fat body cells to actively swim to wounds in an adhesion-independent motility mode associated with actomyosin-driven, peristaltic cell shape deformations that initiate from the cortex of the cell center and extend to the rear of the cell, propelling them forward. These waves occur constantly within fat body cells in unwounded pupae and become highly directed with respect to a wound. Once at the wound, fat body cells start to form lamellipodia that extend around the wound margin, assist hemocytes to clear the wound of cell debris, tightly seal the epithelial wound gap, and release antimicrobial peptides to fight wound infection [38].

Inspired by these recent experimental discoveries of amoeboid mode of swimming—in the strict sense of adhesion-independent cell—fluid interaction that involves large-scale of cell shape deformations, it is timely to conduct a modeling study on chemotaxis driven Dd swimming that allows the coupling of signaling dynamics and biohydrodynamics. In recent years, several models for single cell amoeboid swimming have emerged, many focus on exploring the fluid—structure interaction in the system and how the amoeboid style of shape deformations lead to swimming in various viscous fluid environments [39–45], some also consider the underlying membrane protein kinetics that regulate the excitable dynamics of the cell membrane deformations [46, 47]. In this paper, we

develop a model that includes a deforming Dd amoeboid cell and a group of bacteria, where the amoeboid cell swims following chemoattractant signal produced by the bacteria. The model is a minimal one that couples the chemotaxis dynamics and the hydrodynamic effects. The paper is structured as follows. In section 2 we introduce the model setup, where the active bacterium motions are modeled by a random walk model (section 2.1), the chemotaxis signaling dynamics is numerically solved using the finite volume method in a moving mesh (section 2.2), the Dd amoeboid cell shape deformations and the resulting fluid dynamics are modeled and solved using an established complex analysis technique (section 2.3) [45, 48-50]. Numerical results are presented and discussed in section 3, where we first discussed the chemotaxis guided amoeboid swimming with one bacterium (section 3.1), then how bacterial rheotaxis could help the bacteria escape from the predator Dd cell (section 3.2), finally chemotaxis guided amoeboid swimming with a dilute suspension of bacteria (section 3.3).

2. Modeling framework

In this section we will discuss the development of the model, including the bacterial motions (section 2.1), the chemotaxis dynamics (section 2.2), the deforming Dd cell and the resulting fluid dynamics (section 2.3). We consider a system consisting of a Dd amoeboid cell and bacteria in low Reynolds number incompressible Newtonian fluid. For simplicity of modeling and computation, we will consider a 2D system. Many of the chemotaxis induced Dd cell swimming experiments are performed in containers sufficiently large so as to avoid influences from the walls [36, 37]. In this paper, we also consider a 'large tank' modeling system, where the fluid mechanics resulted mainly from the swimming deformable Dd cells is obtained using the *mathematical amoeba model* [39, 45, 48–50] approach, which provides the solution in a 2D infinite fluid domain (section 2.3); on the other hand, the signaling dynamics is modeled using a movingmesh based reaction-diffusion-convection (RDC) PDE model (section 2.2), where we assume a finite but sufficiently large computation domain for the RDC system. Such a coupled modeling framework allows us to efficiently study the dynamics of the system with relatively low computational costs, assuming the swimming Dd and bacteria are all away from the computational boundary of the RDC submodel.

2.1. Bacterium motions

We consider *Escherichia coli* (*E. coli*) as a representative bacteria model. *E. coli*'s typical movement strategy is well known as run-and-tumble: an *E. coli* can either rotate its flagella counterclockwise resulting in a directed straight 'run', or rebundle its flagella by rotating them clockwise resulting in a 'tumble' which

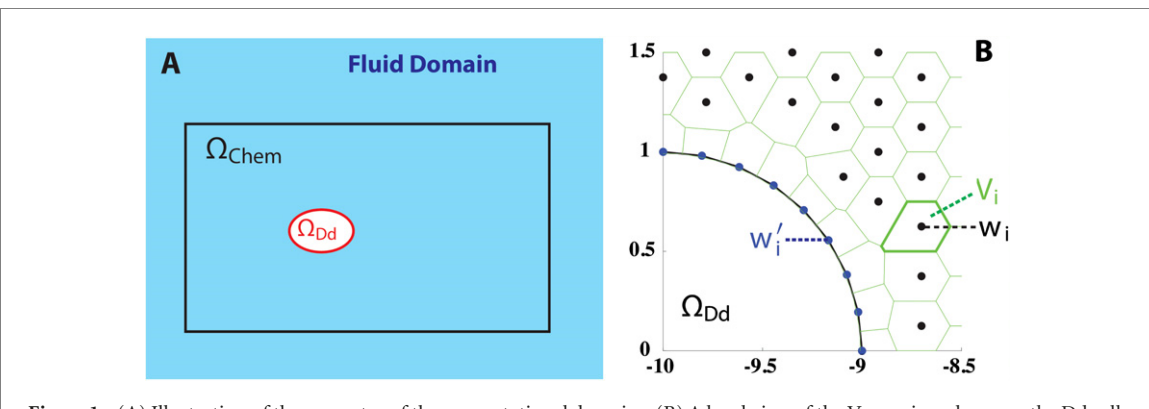


Figure 1. (A) Illustration of the geometry of the computational domains. (B) A local view of the Voronoi meshes near the Dd cell.

reorients the cell without significant change of location [9, 10]. The E. coli constantly switch between the run and tumble modes. The mean run interval is reported to be about 1 s in the absence of chemotaxis, and the mean tumble interval is about 0.1 s, and both are distributed exponentially [11]. In our model system, we will first consider one amoeboid Dd cell with one E. coli, due to the small size of an E. coli (length $\sim 2-3 \mu \text{m}$, diameter $\sim 1 \mu \text{m}$ [51]) compared to that of a Dd cell (length $\sim 22-25 \,\mu\text{m}$, diameter $\sim 4-6 \,\mu\text{m}$ [36, 37]), the E. coli can be well modeled as moving particles without considering the flow stirred by their deformation and movement. Later (section 3.3) we will consider a system of one amoeboid Dd cell with a group of E. coli in a dilute suspension, where the number of E. coli is small (≤ 12) and are separated. In such a dilute suspension scenario, for simplicity, we do not consider the hydrodynamic effects among the E. coli or between the amoeboid Dd cell and an E. coli. However, we point out that if a large amount of E. coli is presented, the active suspension will greatly alter the hydrodynamic effects of the system, causing effects including clustering of E. coli. Refer to the discussion section for potential future extensions.

We start with N_B bacteria in the system, where each bacterium is represented as a dot with its position vector $\mathbf{x}_n = (x_n, y_n), n = 1, 2, ..., N_B$. Without considering the flows generated by the movement of the bacteria, the movement of a bacterium mainly consists of two parts: a convection term of the fluid, and an active movement term from the run-and-tumble. Since the mean tumble interval (~ 0.1 s) is much less than the mean run interval (~ 1 s) [11], we model it as a random walk, where the run is modeled as a jump and the tumble serves a reorientation of the bacterium. The movement of each bacterium is described by the following equation:

$$d\mathbf{x}_n = \mathbf{u}(\mathbf{x}_n)dt + d\mathbf{X}_n,\tag{1}$$

where $\mathbf{u}(\cdot)$ gives the fluid velocity field that is calculated via a complex analysis approach (section 2.3); \mathbf{X}_n denotes the random walk of the bacterium, and we assume that at each small time step dt, the bac-

terium moves a distance δ_J in the direction ϑ_n . In the following discussion we start by considering a 2D random walk of the bacterium, where $\vartheta_n \sim U(-\pi,\pi)$.

Recent research results reveal that bacterial rheotaxis plays a role in bacterial swimming, even without presence of a nearby surface [52]. To computationally investigate the effects of bacterial rheotaxis on bacterial escaping, that is, when the motions of the bacteria are directed in response to the local fluid velocity gradient, we use a hybrid type of random walk model to model the bacterial rheotaxis, where the moving direction ϑ_n is given by the following equation:

$$\vartheta_n = (1 - s_n)\xi_r \pm \left(\arg \mathbf{u}(\mathbf{x}_n) + s_n(1 - s_n)\pi\xi_b\right),$$
(2)

where $s_n = \min(1, \|\mathbf{u}(\mathbf{x}_n)\|/M) \in [0, 1]$ measures the sensitivity of the bacterium to the local fluid velocity with M the cut-off value for the fluid velocity amplitude. $\arg \mathbf{u}(\mathbf{x}_n)$ is the argument of the local fluid velocity, $\xi_{\rm r} \sim U(-\pi,\pi)$ represents the random walk part of ϑ_n , $\xi_b \sim N(0,1)$ and the sum of the two terms $(\arg \mathbf{u}(\mathbf{x}_n) + s_n(1 - s_n)\pi\xi_b)$ represents the correlation with the fluid velocity due to rheotaxis, where we are assume two types of rhoetactic movement—along the flow (+) or against it (-). Equation (2) is an empirical way to model the bacterial rheotaxis, in a way to ensure that (1) when the bacterium is far apart from the Dd cell $(s_n \to 0)$, the bacterium does not sense the flow thus it undergoes a random walk without bias (notice that with $\xi_{\rm r} \sim U(-\pi,\pi)$, we have $\xi_{\rm r} \pm \Theta \sim U(-\pi,\pi)$ for any angle Θ), (2) when the bacterium is near the Dd cell $(s_n \to 1)$, bacterial movement is dominated by rhotaxis ($\vartheta_n = \pm \arg \mathbf{u}(\mathbf{x}_n)$), and (3) bacterial movement continuously change between unbiased and biased random walk depending on s_n .

Comparing to a typical shape deformation cycle of a Dd cell of about $T \sim 1-2$ min [36, 37], the mean run interval is ~ 1 s subjected to exponential distribution [11]. For simplicity, we take the small time step dt of the random walk $d\mathbf{X}_n$ as dt = 0.1T, where T is the average period of a Dd cell swimming cycle.

2.2. Chemotaxis signaling dynamics

Dictyostelium discoideum (Dd) utilizes folic acid receptor 1 (fAR1), a class of single G-protein-coupled receptor (GPCR) to detect diffusible chemoattractant folate secreted by bacteria, thus to locate and chase bacteria [53]. Once the amoeba 'catches' the bacteria, the amoeba engulfs and consumes them. Dd amoeboid cell is reported to ingest, kill and digest bacteria at a rate of at least one per minute [54].

Suppose that at time t, the amoeboid cell captures a region $\Omega_{\mathrm{Dd}}(t)$ in the 2D infinite domain, thus Ω_{Dd}^{C} , $\partial\Omega_{\mathrm{Dd}}$ give the external fluid domain and the cell boundary, respectively. Let $f(\mathbf{x},t)$, $R_{f}^{0}(\mathbf{x},t)$ and $R_{f}(\mathbf{x},t)$ denote the concentration of diffusive folate, the surface concentration of free fAR1 receptors and the surface concentration of the folate-bond fAR1 receptors, respectively. $f(\mathbf{x},t)$ is defined on $\Omega_{\mathrm{Dd}}^{C}(t) \times [0,\infty)$ and $R_{f}^{0}(\mathbf{x},t)$, $R_{f}^{0}(\mathbf{x},t)$ are defined on $\partial\Omega_{\mathrm{Dd}}(t) \times [0,\infty)$. The signaling dynamics of the diffusible chemoattractant folate and the fAR1 receptors on the cell membrane are modeled by the following RDC equations together with boundary conditions:

$$\frac{\partial f}{\partial t} = D\Delta f - \mathbf{u} \cdot \nabla f$$

$$+ a \int \sum_{n=1}^{N_{\rm B}} \delta(\mathbf{x} - \mathbf{x}_n) d\mathbf{x} \quad \text{in } \Omega_{\rm Dd}^{C}(t) \quad (3)$$

$$D\frac{\partial f}{\partial n} = -k_{+}fR_{f}^{0} + k_{-}R_{f} \quad \text{on } \partial\Omega_{\mathrm{Dd}}(t)$$

$$\frac{\partial R_{f}}{\partial t} = k_{+}fR_{f}^{0} - k_{-}R_{f} - \gamma R_{f}$$

$$+ \varsigma R_{f}\frac{\mathrm{d}W}{\mathrm{d}t} \quad \text{on } \partial\Omega_{\mathrm{Dd}}(t)$$
(5)

with the constraints:

$$R_f^0(\mathbf{x},t) + R_f(\mathbf{x},t) = R_{\text{max}}$$
,
$$f(\mathbf{x},t) \ge 0, R_f^0(\mathbf{x},t) \ge 0, R_f(\mathbf{x},t) \ge 0.$$

The terms in equations (3)–(5) are explained as follows.

- $D\Delta f$: diffusion of folate with the diffusion rate D.
- $\mathbf{u} \cdot \nabla f$: convection of folate, where \mathbf{u} gives the velocity field of the extra-cellular flow.
- $a \int \sum \delta d\mathbf{x}$: production of folate molecules from the bacteria, where a is the folate production rate. For simplicity, we assume that all bacteria have the same folate production rate.
- $k_+fR_f^0$, k_-R_f : biochemical reactions between folate molecules and fAR1 receptors along the cell membrane boundary, where k_+ , k_- are the binding and unbinding rates of the fAR1 receptors. R_{max} is the sum of free and folate-bond receptors, and we assume it a constant along the cell boundary.
- γR_{j} : degradation of folate-bond fAR1 receptors, where γ is the degradation rate.

• $\varsigma R_f dW$: white noise that captures stochastic effects in intracellular signal dynamics, where ς is the noise strength.

Computationally, instead of considering the infinite fluid domain, we consider a finite but large enough computational domain $\Omega_{\rm Chem}$ that contains the cell domain $\Omega_{\rm Dd}$ and all the bacteria, and ${\rm Area}(\Omega_{\rm Dd}) \ll {\rm Area}(\Omega_{\rm Chem})$ (illustrated in figure 1(A)). Therefore the fluid domain boundary consists of two pieces: $\partial\Omega_{\rm Dd}$ and $\partial\Omega_{\rm Chem}$. We assume no-flux Neumann boundary condition $\hat{\bf n}\cdot\nabla f=0$ on $\partial\Omega_{\rm Chem}$.

To solve the RDC equations (3)–(5), we use the Voronoi tessellation based finite volume method formulated in [55, 56]. Initially, we generate a network of fluid 'nodes' $\{\mathbf{w}_i\}$ in the computational fluid domain $\Omega_{\mathrm{Chem}} \cap \Omega_{\mathrm{Dd}}^{C}$, and discretize the cell boundary $\partial \Omega_{\mathrm{Dd}}$ by N_{R} nodes $\mathbf{w}_0', \mathbf{w}_1', \ldots, \mathbf{w}_{N_{\mathrm{R}}}' = \mathbf{w}_0'$ —how to choose the discretization will be discussed in section 2.3. Notice that the positions of both the boundary nodes $\{\mathbf{w}_i'(t)\}$ and $\{\mathbf{w}_i(t)\}$ change as the Dd cell deforms and perturbs the surrounding fluid. At each computational time step, the fluid nodes $\{\mathbf{w}_i\}$ are updated as

$$\mathbf{w}_i^{n+1} = \mathbf{w}_i^n + \mathbf{u}(\mathbf{w}_i^n) \Delta t, \tag{6}$$

where \mathbf{u} is the fluid velocity field. We generate a Voronoi tessellation $\{V_i^{n+1}\} \cup \{V_i'^{n+1}\}$ of the computational domain $\Omega_{\mathrm{Chem}} \cap \Omega_{\mathrm{Dd}}^{C}$ based on the nodes $\{\mathbf{w}_i^{n+1}\} \cup \{\mathbf{w}_i'^{n+1}\}$, that is, V_i^{n+1} (or $V_i'^{n+1}$) is the set of all the points in the computational fluid domain $\Omega_{\mathrm{Chem}} \cap \Omega_{\mathrm{Dd}}^{C}$ closer to the node \mathbf{w}_i (or \mathbf{w}_i') than any other node (figure 1(B)).

The folate concentration data f is available at the nodes $\{\mathbf{w}_i\}$. In the Lagrangian frame, the convection term $\mathbf{u} \cdot \nabla f$ disappears from equation (3). The Laplacian in equation (3) can thus be approximated for each Voronoi tile V_i through summation of the fluxes across the edges partitioning V_i from each of its Delaunay neighbors (denoted by Λ_i) [55]:

$$\Delta f_{i} \approx \frac{1}{\operatorname{Area}(V_{i})} \int_{\partial V_{i}} \mathbf{n} \cdot \nabla f ds$$

$$\approx \frac{1}{\operatorname{Area}(V_{i})} \sum_{i \in \Lambda_{i}} \frac{f_{j} - f_{i}}{\|\mathbf{w}_{j} - \mathbf{w}_{i}\|} l_{ij}$$
(7)

,where $f_i = f(\mathbf{w}_i)$, and l_{ij} is the length of the common edge shared by V_i and V_j . Notice that for a Voronoi tile V_i , its Delaunay neighbors may also include Dd cell boundary tiles V_i' , but for simplicity, we omit the notation ' in equation (7). Numerical convergence studies show that the method converges linearly in the L^2 norm [57]. We solve equation (3) numerically in a forward Euler scheme, with the Laplacian approximated by equation (7). Equation (3) can be numerically solved as follows:

$$f_i^{n+1} = f_i^n + \left(D\Delta f_i^n + \frac{a\sum_{n=1}^{N_{\rm B}} \delta_{V_i}(\mathbf{x}_n)}{\operatorname{Area}(V_i)} \right) \Delta t,$$

Figure 2. Shapes of the Dd cell in a cycle, showing the polarization, swimming and relaxation phases. Arrows indicate the cellular polarization direction θ within the cycle. At the end of the cycle, a new direction is selected.

where $\delta_{V_i}(\mathbf{x}_n) = 1$ if the *n*th bacteria is in V_i , otherwise $\delta_{V_i}(\mathbf{x}_n) = 0$.

For boundary conditions, first we notice that while other nodes \mathbf{w}_i locates inside the corresponding Voronoi tile V_i , the cell boundary nodes \mathbf{w}_i' locate on $\partial V_i' \cup \partial \Omega_{\mathrm{Dd}}$ (figure 1(B)). To each cell boundary \mathbf{w}_i' , the numerical Laplacian equation (7) can be modified as:

$$\Delta f_i \approx \frac{1}{\operatorname{Area}(V_i')} \left(\sum_{j \in \Lambda_i} \frac{f_j - f_i}{\|\mathbf{w}_j - \mathbf{w}_i'\|} l_{ij} + (\mathbf{n} \cdot \nabla f) l_i' \right),$$
(8)

where we approximate the boundary $\partial V_i \cap \partial \Omega_{\mathrm{Dd}}$ by a line segment connecting the two vertices shared by neighboring Voronoi tiles, and let l_i' be its length. For boundary condition on $\partial \Omega_{\mathrm{Dd}}$ given by equation (4), along the small boundary segment $\partial V_i' \cap \partial \Omega_{\mathrm{Dd}}$ we have:

$$\frac{\partial f}{\partial n} = \mathbf{n} \cdot \nabla f = \frac{1}{D} \left(-k_+ f R_f^0 + k_- R_f \right)$$

and equation (8) becomes:

$$\Delta f_i pprox rac{1}{ ext{Area}(V_i)} \left(\sum_{j \in \Lambda_i} rac{f_j - f_i}{\|\mathbf{w}_j - \mathbf{w}_i'\|} l_{ij}
ight. \ + rac{l_i^M}{D} \left(-k_+ f R_f^0 + k_- R_f
ight)
ight).$$

Finally, the no-flux boundary condition on $\partial\Omega_{\text{Chem}}$ can be directly enforced to equation (8).

2.3. Chemotaxis induced Dd shape deformations and swimming

When adhesion is absent thus cell crawling is disabled, Dd cells can swim towards a chemoattractant source. During swimming, cells form pseudopods that convert to rear-ward moving bumps thereby propelling itself through the surrounding fluid in a totally adhesion-free fashion [7, 36, 37, 58]. Such a swimming mode is very different from ciliated or flagellated swimming modes that are commonly adopted by many bacteria including *E. coli*, as it is the one that requires large deformations that propagate over the cell body. We use the *mathematical amoeba model* [39, 45, 48–50] to generate the Dd cell deformation as well as to solve the resulting cell–fluid interaction.

In the following we list the outline of the modeling framework, see the supplement for more details (https://stacks.iop.org/PB/18/045001/mmedia).

Consider the following conformal mapping defined from $\{\zeta \in \mathbb{C}; |\zeta| \geqslant 1\}$ to $\Omega_{\mathrm{Dd}}^{\mathcal{C}}$:

$$w(\zeta;t) = e^{i\theta(t)} \left[r(t)\zeta + \frac{\eta_{-1}(t)}{\zeta} + \frac{\eta_{-2}(t)}{\zeta^2} \right] + Z_{\text{Dd}}(t),$$
(9)

where the Dd cell shape is defined by $\partial\Omega_{\mathrm{Dd}}(t) = \{w(\sigma;t)|\sigma\in S^1\}$. The N_{r} discretization nodes $\{\mathbf{w}_1',\mathbf{w}_2',\ldots,\mathbf{w}_{N_{\mathrm{r}}}'\}$ are generated as follows: we discretize the unit circle ∂D in the computational ζ -plane equally into N_{r} nodes:

$$\sigma_i = e^{i\theta_j} = e^{i\frac{2\pi j}{N_r}}, \quad j = 0, 1, 2, \dots, N_r - 1$$

then let $\mathbf{w}_i' = w(\sigma_i; t)$. In equation (9), $\theta(t) \in \mathbb{R}$ gives the cell polarization that will be determined by signaling sensing dynamics as discussed below. The swimming Dd cell undergoes cyclic shape deformation with the same period T. We assume that the polarization θ is determined at the beginning of a swimming cycle and will not change during the cycle, thus $\theta(nT + t) \equiv \theta(nT)$ for $t \in [0, T)$. $r, \eta_{-1}, \eta_{-2} \in \mathbb{R}$ control the cell size and shape deformations, and are subjected to area conservation of the cell. $Z_{Dd}(t)$ gives the location of the cell, while $U_{\rm Dd}(t) = Z_{\rm Dd}(t)$ gives the velocity of the cell and is computed from the Goursat formula [59]. The fluid velocity field u, or in the complex notation u, can be also obtained through the Goursat formula. Refer to supplement section 1 for more details of the complex analysis techniques involved in this part.

We assume that the Dd cell undergoes shape deformations in response to signal gradient, with each swimming cycle lasting for a period of T and consisting of three phases: (i) polarization, when the Dd cell determines the polarization θ during the current cycle in response to the signal R_f , and elongates its cell body in preparation for (ii) swimming, when the Dd cell deforms its shape so to actively swim along the polarization direction, followed (iii) relaxation, when the Dd cell returns to its initial circular shape. Durations of polarization and relaxation phases are chosen to be much shorter than the swimming phase. Figure 2 shows a typical cycle of the Dd cell shape deformations. For more details of the modeling setup of

IOP Publishing *Phys. Biol.* **18** (2021) 045001 Q Wang and H Wu

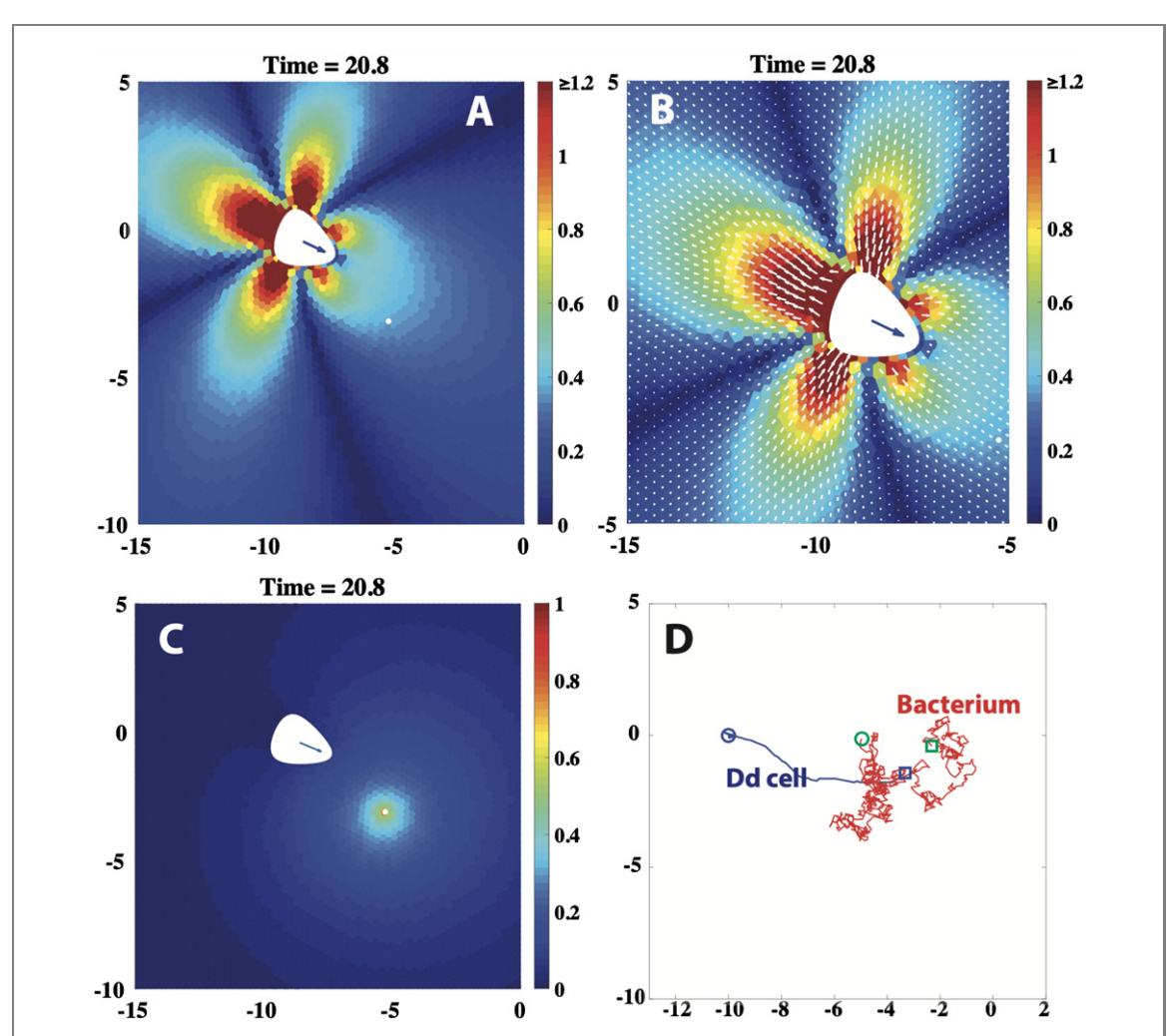


Figure 3. Simulation of a swimming Dd cell following a bacterium guided by chemotaxis. (A) and (B) Snapshots of the fluid velocity at T = 20.8, where the heatmap (B) shows the amplitude of the fluid velocity, in the zoom in view near the Dd cell (C), the white arrows show the fluid velocity directions. (C) A snapshot of the heatmap of the diffusive folate signal concentration at T = 20.8. In (A)–(C), both the Dd cell and the bacterium are colored in white. (D) trajectories of the Dd cell (blue) and the bacterium (red), where circles show the start points of the Dd cell center (blue circle) and the bacterium (green circle), and squares show the end points of the Dd cell center (blue square) and the bacterium (green square). The Dd cell catches the bacterium after 69 swimming cycles.

the signaling induced Dd cell polarization and shape deformations, please refer to supplement section 2.

In our model, we do not model the engulfment process in phagocytosis. For simplicity, once a bacterium falls within a close enough distance near a cell boundary node \mathbf{w}_j' , we consider it taken by the amoeba and remove it from the system.

2.4. Computations of the model

We nondimensionalize the system, using the duration of a Dd cell swimming cycle T and the radius of a Dd cell at rest r_0 as the characteristic temporal and spatial scales, and $R_{\rm max}$ the characteristic concentration scale for f and R_f . The non-dimensionalized system can be found in supplement section 3.

The system is computed using the following update algorithm:

(a) **Signaling dynamics.** Generate the Voronoi tessellation from the current distribution of 'nodes' $\{\mathbf{w}_i\} \cup \{\mathbf{w}_i'\}$. Update f and R_f by solving the RDC

equations using the finite volume method in the moving mesh.

(b) Dd amoeboid cell shape.

- 1. If the cell is at rest in a circular shape $(t = nT, n \in \mathbb{N})$, determine the cell polarization θ for this swimming cycle.
- 2. **ElseIf** the cell is during a swimming cycle, $t \in (nT, (n+1)T), n \in \mathbb{N}$, update the conformal mapping w equation (9).
- (c) **Fluid mechanics.** Update flow velocity field **u** from the Goursat formulas. Update bacteria positions and the moving mesh:
 - 1. **Bacteria motions.** Update bacterial positions by equation (1). Remove any bacterium that comes to cell boundary Voronoi tiles.
 - 2. **Moving mesh.** Update the moving mesh nodes $\{w_i\}$ from equation (6).

The numerical scheme works for our model system where hydrodynamics and signaling dynamics

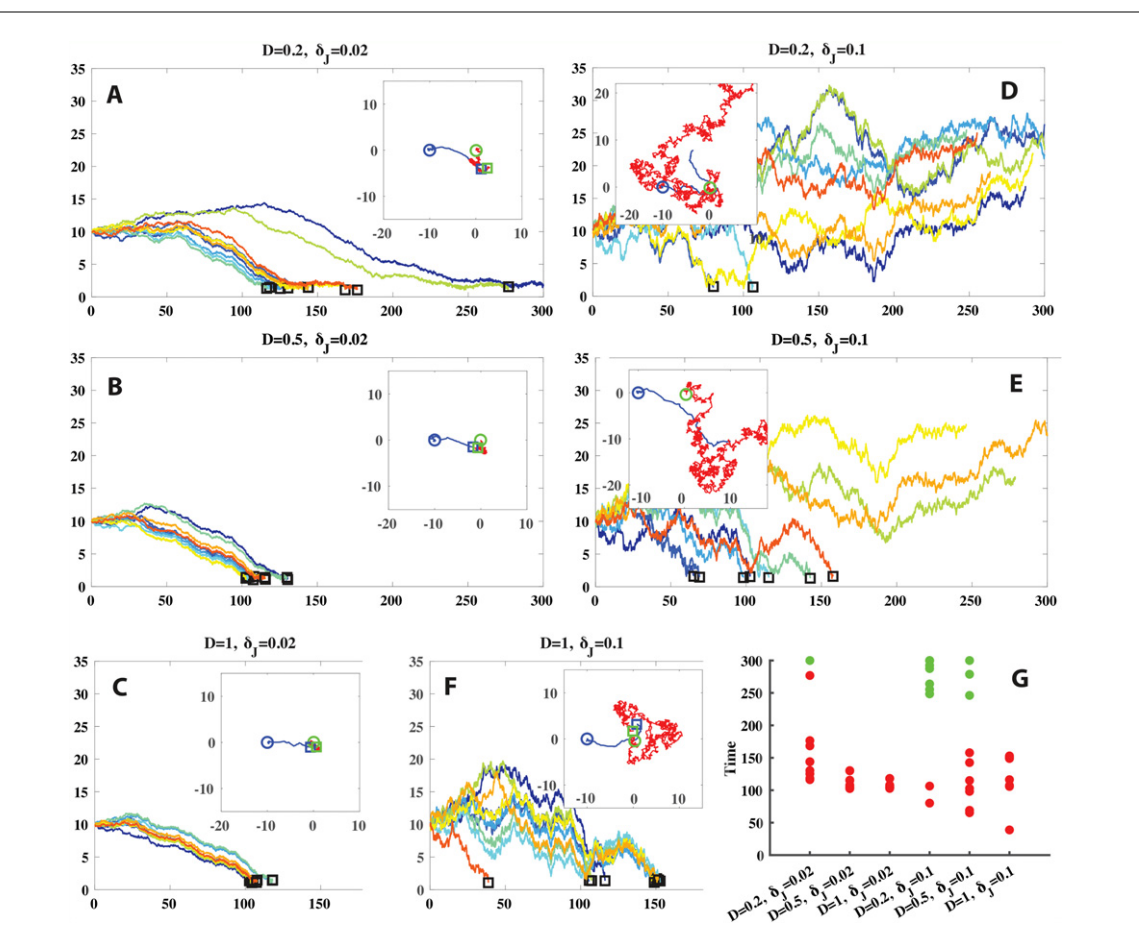


Figure 4. Simulation results of chemotaxis guided Dd cell swimming. (A)–(F) Distance between the Dd cell center and the bacterium with different combinations of D and δ_I values. x-axis shows the time counted as swimming cycles. Each colored curve shows the result from one simulation from the group, and black boxes show when the Dd cell catches the bacterium. The sub-panel in each panel shows the trajectories of the Dd cell (blue curve) and the bacterium (red curve) from one typical simulation from the group, with the blue and green circles mark the starting locations of the Dd cell and the bacterium, and the blue and green squares mark the end locations of the Dd cell and the bacterium when the Dd cell catches the bacterium. (G) Durations of the simulations, where red dots show when the Dd cell catches the bacterium, green dots show when the bacterium runs out of Ω_{Chem} : $[-25,25] \times [-25,25]$, or the Dd cell does not catch the bacterium by the end of 300 cycles.

are coupled, and allows us to study cellular chemotaxis and rheotaxis in a fluid environment. We point out that we do see fluid nodes near the Dd cell boundary getting closer after many swimming cycles due to the large deformation of the cell, which causes numerical instability of the finite volume method. We solve this numerical issue by a local re-mesh near the Dd cell, see more details in supplement section 4. Parameter values used in our simulations are given in supplement table 1.

3. Results

3.1. Chemotaxis guided amoeboid swimming allows the Dd amoeboid cell to follow and catch bacteria

We start with a system consisting of one Dd cell and one bacterium where the bacterium undergoes an unbiased random walk (equation (1)). Simulation results show that the Dd amoeboid cell is able to swim following the bacterium guided by the chemoattractant signal. Figure 3 shows a typical simulation, where

the Dd cell catches the bacterium after 69 cycles. Compared to the random walk of the bacterium, the motion of the Dd cell is more directed; as the Dd cell approaches the bacterium, the bacterium is pushed away to the right by the flow generated by the swimming Dd cell, and eventually being captured by the Dd cell (figure 3(C)). The full time lapse snapshots of the fluid velocity profile during one Dd cell swimming cycle is provided in supplement figure 2.

We consider how the chemoattactant diffusion rate D and the bacterial jump amplitude δ_I affect the Dd cell swimming dynamics. We perform 6 groups of 10 simulations, with different values of D and δ_I : $D=0.2,0.5,1,\delta_I=0.02,0.1$. Simulations results show large coefficient rate D makes it easier for the Dd cell to follow the signal guidance thus catch the bacterium; bacterial random walk strength δ_I may also help the bacterium to escape, however, the more important effect of δ_I is that it increases the variance of time for the Dd cell to catch the bacterium, if it could (figure 4). The increase of catch time variance needed caused by δ_I should not be surprising, since the passive motion of the

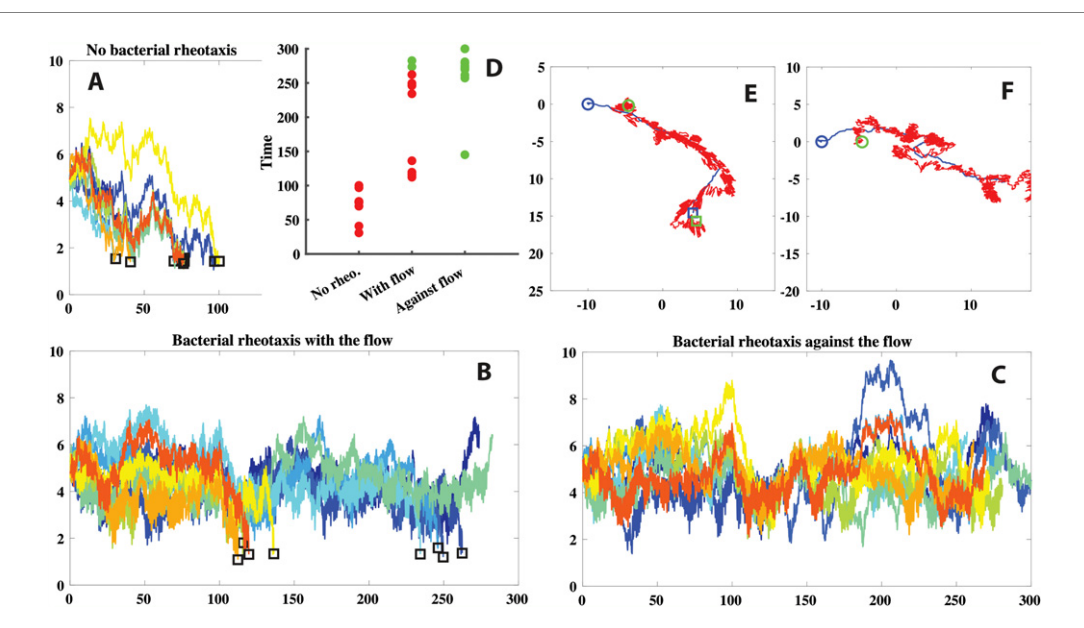


Figure 5. Simulation results of bacterial rheotaxis. (A)–(C) Distance between the bacterium and the Dd cell center with (A) no bacterial rheotaxis, (B) bacterial rheotaxis with the flow, and (C) bacterial rheotaxis against the flow. x-axis shows the time counted as swimming cycles. Each colored curve shows the result from one simulation from the group, and black boxes in (A)–(C) show when the Dd cell catches the bacterium. (D) Durations of the simulations, where red dots mark the time when the Dd cell catches the bacterium, green dots mark when the bacterium runs out of $\Omega_{\rm Chem}$: [-25,25] × [-25,25], or the Dd cell does not catch the bacterium by the end of 300 cycles. (E) Trajectories of the Dd cell (blue curve) and the bacterium (red curve) with bacterial rheotaxis with the flow, with the blue and green circles mark the starting locations of the Dd cell and the bacterium, and the blue and green squares mark the end locations of the Dd cell and the bacterium when the Dd cell catches the bacterium. (F) Trajectories of the Dd cell (blue curve) and the bacterium (red curve) with bacterial rheotaxis against the flow, with the blue and green circles mark the starting locations of the Dd cell and the bacterium, the Dd cell does not catch the bacterium in 300 cycles.

bacterium is an unbiased random walk X, thus $E(\mathbf{X}) = 0$ and large δ_I only increases $Var(\mathbf{X})$ which in return increases the catch time variance, though through a complex chemotaxis induced amoeboid swimming dynamics. Figure 4 shows that in 10 out of 10 simulations with D = 0.5, $\delta_I = 0.02$ (figure 4(C)) $D = 1, \delta_I = 0.02$ (figure 4(C)) or $D = 1, \delta_I = 0.1$ (figure 4(F)), the Dd cell is able to catch the bacterium within 300 cycles, compared to 9 out of 10 with D = 0.2, $\delta_I = 0.02$ (figure 4(A)) and 7 out of 10 with D = 0.5, $\delta_I = 0.1$ (figure 4(E)). The worst scenario for the Dd cell is small D and large δ_I : with $D = 0.2, \delta_I = 0.1$, only in 2 out of 10 simulations the Dd cell catches the bacterium within 300 cycles (figure 4(D)). In the above simulations we take $k_{-}=0$, finally we take $k_{-}=0.1$ and with D=0.5, $\delta_I = 0.02$, the results from 10 simulations are shown in supplement figure 3, compare with $k_- = 0$ (figure 4(B)), which indicates that large k_{-} helps the bacterium to escape from the Dd cell.

We present the time lapse snapshots from typical simulations with $\delta_J = 0.1, D = 0.2, 0.5, 1$ in supplement figures 4–6.

3.2. Rheotaxis helps bacteria escaping from the predator

Next, we use the model to investigate if rheotaxis could help the bacterium run away from the predator Dd cell. In particular, we consider two types of bacterial rheotaxis: the bacterium prefers to move with

the flow vs against the flow. We model either of the two rheotactic systems by a biased random walk of the bacterium, where the direction of the bacterium's jump ϑ is given by equation (2), and it takes the + sign if the bacterium prefers to move with the flow, and the - sign if against the flow.

We performed three groups of simulations: (1) no bacterial rheotaxis, (2) bacterial rheotaxis with a biased random walk with the flow, and (3) bacterial rheotaxis with a biased random walk against the flow. We take D = 1, $\delta_I = 0.05$ in all three groups, and in each group we run 10 simulations. Simulation results are shown in figure 5. Without bacterial rheotaxis, the Dd cell catches the bacterium in all 10 simulations (figures 5(A) and (D)). With bacterial rheotaxis with the flow, in 8 out of 10 simulations it needs longer time for the Dd cell to catch the bacterium and 8 out of 10, and in the other 2 simulations the bacterium runs out of the $\Omega_{\rm Chem}$ domain after >250 Dd cell swimming cycles (figures 5(B) and (D)). Finally with bacterial rheotaxis against the flow, in 8 out of 10 simulation the bacterium runs out of the Ω_{Chem} domain, and in the other 2 simulations the bacterium stays within the Ω_{Chem} domain always but the Dd cell does not catch the bacterium in 300 cycles (figures 5(C) and (D)). Figure 5(E) shows the trajectories of the Dd cell and the bacterium with bacterial rheotaxis with the flow from one simulation, when the Dd cell catches the bacterium at the end, and figure 5(F) shows the trajectories of the Dd cell and the bacterium

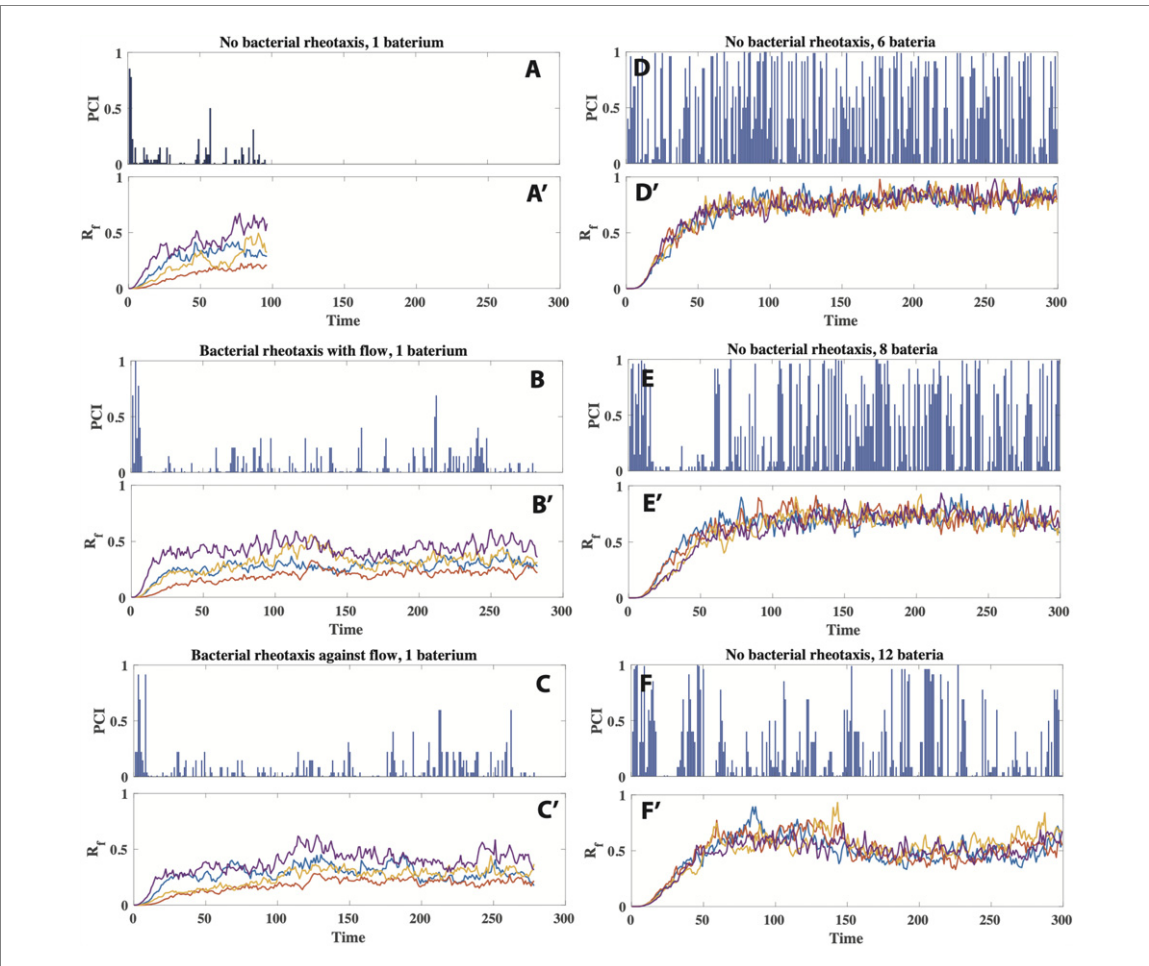


Figure 6. Dd cell polarization change. Each top panel (A)–(F) shows the PCI changes in one simulation with the conditions shown by the panel title, and the bottom panels (A')–(F') shows the R_f concentration at four sites along the Dd cell boundary, with each neighboring pair separated by an angle of $\pi/2$. (A) and (A'), (B) and (B'), (C) and (C') show a more directed Dd cell swimming when guided by a single bacterium, whether with or without bacterial rheotaxis. (D) and (D'), (E) and (F') and (F') show a more chaotic Dd cell swimming when surrounded by more bacteria.

with bacterial rheotaxis against the flow from another simulation, the Dd cell does not catch the bacterium in 300 cycles.

Our simulation results (figure 5) show that while bacterial rheotaxis against the flow appears to be a good strategy for the bacterium to escape from the predator Dd cell, bacterial rheotaxis with the flow may also help the bacterial to run away a little compared to no rheotaxis. We emphasize that at LRN, since inertia is absent, the current flow profile only depends on the current Dd cell deformation, and it keeps changing over a swimming cycle (see supplement figure 2). The bacterial rheotaxis we find here is the result out of one or even multiple Dd cell swimming cycles. Moreover, we would also point out that even in the best simulated scenario—bacterial rheotaxis against the flow, the bacterium is not able to fully escape from the Dd cell, which can be seen from figure 5(C) that the distance between the Dd cell and the bacterium oscillates but the mean is not increasing, indicating that the Dd cell keeps following the bacterium.

3.3. Chemotaxis guided amoeboid swimming caused by a dilute suspension of bacteria

Finally we consider the system with one Dd cell and a dilute suspension of bacteria, that is, a small number of bacteria present in the system. In the dilute suspension, the hydrodynamic interactions among the bacteria can be ignored. We consider systems where initially a group of N bacteria locate equispaced in a ring with the Dd cell center as the ring center (see supplement movie and supplement figures 7–9, the color scales are the same as figure 3(C)), and D=1, $\delta_I=0.1$ in all simulations in this section.

Simulations results show that similar to the systems with only one bacterium, when multiple bacteria are present, the Dd cell is still able to follow the chemoattractant signals and catch some bacteria. However, we notice that unlike in the systems with only one bacterium where the Dd cell movement is more directed, now with more bacteria present, the movement of the Dd cell becomes more chaotic—the Dd cell changes its polarization between consecutive

cycles more frequently. To quantify this effect, we define a Dd cell polarized orientation change index PCI as follows:

$$PCI_n = \frac{1 - \cos(\theta_n - \theta_{n-1})}{2}, \quad n \geqslant 2, \ n \in \mathbb{N},$$

where PCI_n denotes the PCI for the nth swimming cycle $t \in [nT, (n+1)T)$, and θ_n is the Dd cell polarization angle in the nth cycle. PCI_n takes values in [0,1], with $PCI_n = 0$ means that the polarization does not change between the two consecutive cycles, while $PCI_n = 0$ means that the polarization changes with an angle π , i.e. the polarization is reversed.

We compare simulation results between systems with one bacterium only and systems with multi bacteria, the former group includes single bacterium with no external flow (figures 6(A) and (A')), single bacterium with rheotaxis along the flow (figures 6(B) and (B')) and against the flow (figures 6(C) and (C')), and the latter multi bacteria group includes 6, 8 or 12 bacteria with no external flow (figures 6(D) and (D'), (E) and (E'), (F) and (F')). In the initial stage of all the simulations, the chemoattractant signal has not diffused to the whole Dd cell, causing a random polarization of the cell. Therefore, PCI is high in a small period at the beginning stage. After the initial stage, the Dd cell is able to receive the diffusive chemoattractant signal. In the systems (no rheotaxis, rheotaxis along and against the flow) with only one bacterium, the averagely low PCI indicates that the Dd cell performs a more directed swimming toward the bacterium (figures 6(A)–(C)). On the other hand, PCI is averagely high when more bacteria are present, indicating that the polarization decision of the Dd cell is affected by many body effect, and thus presents a chaotic behavior without the ability to effectively follow and catch a bacterium. Looking further into the dynamics of the chemotaxis guided amoeboid swimming (supplement movie and supplement figures 7-9), we find that the number multiplication of bacteria plays a similar role as the period multiplication as a road transition to the chaos [60]. Due to the Dd cell surrounded by multiple strong signal sources, the polarization of the Dd cell is frequently changed. In each of simulations in 6, we track the R_f concentrations at four sites along the Dd cell boundary, with each neighboring pair separated by an angle of $\pi/2$, and the results are given in the bottom panels in figures 6(A')-(F'). With only one bacterium in the system (figures 6(A')-(C')), R_f at the four sites are averagely low (mostly below 0.6), and it is clear that which site is at the front/rear, as its R_f keeps the highest/lowest all the time (purple/orange line in figures 6(A')-(C')). Such a clear difference in the R_f level indicates a clear polarization of the Dd cell. On the other hand, when more bacteria are presented in the system, R_f levels are much higher (figures 6(D')-(F')), and there is no clear high/low difference in the R_f at the four sites

due to the high level as well as noise, leading to the frequent change in the cell polarization as is shown by the PCI plots. This causes the chaotic swimming pattern and reduces the cell's efficiency in catching bacteria. As pointed out above, this chaotic polarization behavior becomes more evident with more bacteria present in the system, which is verified by larger average PCIs in figure 6(F) compared to figures 6(D) and (E).

4. Discussion

While Dd amoeboid cell has long been well known as a model system for chemotaxis study on a crawling based motion, in recent year, Dd cell swimming induced by different types of taxis including chemotaxis has become an emerging research area. A major modeling challenge in this direction is the coupling of signaling dynamics and hydrodynamics. In this paper, we developed a minimal modeling framework to investigate the chemotaxis induced amoeboid cell swimming. Our model captures the interactions between a Dd cell and bacteria, where both biochemical (chemotaxis signaling dynamics) and biomechanical (amoeboid swimming and bacterial rheotaxis) are considered. For the numerical computations, a complex analysis technique—mathematical amoeba model [39, 45, 48-50] is applied to solve the amoeboid dynamics in 2D viscous flows, associated with the finite volume method based on the moving mesh Voronoi tessellation [55, 56] to solve the RDC equation system. Our simulations results show that chemotaxis effectively guides Dd cell swimming, especially when less bacteria are presented in the system, and bacterial rheotaxis may help a bacterium to escape from a predator Dd cell.

To better investigate the dynamics of chemotaxis induced amoeboid cell swimming, there are many aspects that our model can be developed. We discuss some major aspects in the following.

Intracellular signaling dynamics induced amoeboid cell shape deformations. In this paper, we used the 2D mathematical amoeba model (section 2.3), which was greatly used in modeling study of amoeboid cell swimming. However, the shape deformations in the mathematical amoeba model is prescribed. In the future, we plan to develop an intracellular submodel for the amoeboid cell to capture how the membrane protein dynamics in response to extracellular stimuli generates excitable traveling waves of cell shape deformations. Several modeling approaches to this directions have been developed, including models with a phenomenological description of membrane protein reaction-diffusion system that generates excitable dynamics of cell membrane deformation [46, 47] and a crawling based chemotaxis induced amoeboid cell deformation and migration model [61]. We would like to mention that the modeling framework developed in this paper

is compatible with more complex cell deformations, using the computational method developed in [39].

Chemotaxis induced amoeboid swimming in confined space. Currently in our model, we consider a swimming system in free space. However, amoeboid motion generally occurs close to surfaces, in small capillaries or in extracellular matrices of biological tissues. In addition, micro-organisms swim through permeable boundaries, cell walls, or microvasculature. For example, flows are ubiquitous in human immune systems, blood vessels and microcirculation system, and are subjected to biological confinement by complex geometric structures. In particular, the effect of walls on motile micro-organisms has been a topic of increasingly active research. Recently, theoretical and modeling studies have revealed complicated swimming trajectories with the confinement effects and simulation predictions have been verified by experiments [40, 41, 62, 63]. In the future we will develop our model to study a swimming system in confined space.

Hydrodynamic interactions and chemotaxis of bacteria. In this paper we consider only a dilute suspension of bacteria, and we neglect bacterium-bacterium and bacterium-Dd cell hydrodynamic interactions. Due to the large size ratio of the Dd cell to a bacterium, the hydrodynamic effects generated by a bacterium should not affect much of the Dd cell swimming dynamics, yet the hydrodynamic interactions between bacteria might play an important role to bacterial swimming as well as the chemotaxis dynamics when the concentration of bacteria is higher. In recent years, both modeling and experimental studies reveal that in an active suspension of bacteria, hydrodynamics affects bacterial collective motions with chemotaxis [64, 66-69]. Another important future direction to our current modeling study would thus be to consider an active suspension of bacteria with hydrodynamic interactions.

In addition, it is well known that *E. coli* also respond to chemotactic signals, either produced by themselves or following local chemical gradients [65, 69, 70]. Yet whether bacterial chemotaxis play a role in the Dd–*E. coli* swimming system stays unclear. Would bacterial chemotaxis help *E. coli* to run away from the Dd cell is another interesting question to be considered and investigated, on both experimental and modeling sides. In particular, two crucial questions should be addressed: will the Dd send the signal to repel/attract the *E. coli*? With a large amount of *E. coli* presented in the system, how will the chemotaxis induced bacterial clustering alter the Dd–*E. coli* interaction?

Acknowledgments

The authors acknowledge support from the National Science Foundation Grant DMS-1951184 to QW. Computations were performed using the computer clusters and data storage resources of the HPCC, which were funded by grants from NSF (MRI-1429826) and NIH (1S10OD016290-01A1).

Data availability statement

The data that support the findings of this study are available upon reasonable request from the authors.

ORCID iDs

Qixuan Wang https://orcid.org/0000-0003-2673-921X

Hao Wu https://orcid.org/0000-0003-1458-6930

References

- [1] Delanoë-Ayari H, Iwaya S, Maeda Y T, Inose J, Rivière C, Sano M and Rieu J-P 2008 Changes in the magnitude and distribution of forces at different Dictyostelium developmental stages *Cell Motil. Cytoskelet.* 65 314–31
- [2] Sokolov A, Apodaca M M, Grzybowski B A and Aranson I S 2010 Swimming bacteria power microscopic gears *Proc. Natl* Acad. Sci. 107 969–74
- [3] Riedel I H, Kruse K and Howard J 2005 A self-organized vortex array of hydrodynamically entrained sperm cells *Science* 309 300–3
- [4] Lauga E, DiLuzio W R, Whitesides G M and Stone H A 2006 Swimming in circles: motion of bacteria near solid boundaries *Biophys. J.* 90 400–12
- [5] Rafaï S, Jibuti L and Peyla P 2010 Effective viscosity of microswimmer suspensions *Phys. Rev. Lett.* 104 098102
- [6] Manahan C L, Iglesias P A, Long Y and Devreotes P N 2004 Chemoattractant signaling in Dictyostelium discoideum Annu. Rev. Cell Dev. Biol. 20 223–53
- [7] Howe J D, Barry N P and Bretscher M S 2013 How do amoebae swim and crawl? PLoS One 8 e74382
- [8] Bray D 2000 Cell Movements: From Molecules to Motility (New York: Garland Science)
- [9] Stewart R C and Dahlquist F W 1987 Molecular components of bacterial chemotaxis Chem. Rev. 87 997—1025
- [10] Block S M, Segall J E and Berg H C 1982 Impulse responses in bacterial chemotaxis Cell 31 215–26
- [11] Berg H C 1990 Bacterial microprocessing Cold Spring Harbor Symp. on Quantitative Biology (Cold Spring Harbor Laboratory Press) pp 539–45
- [12] Paluch E, Piel M, Prost J, Bornens M and Sykes C 2005 Cortical actomyosin breakage triggers shape oscillations in cells and cell fragments *Biophys. J.* 89 724–33
- [13] Tinevez J-Y, Schulze U, Salbreux G, Roensch J, Joanny J-F and Paluch E 2009 Role of cortical tension in bleb growth Proc. Natl Acad. Sci. 106 18581–6
- [14] Kay R R 2002 Chemotaxis and cell differentiation in Dictyostelium Curr. Opin. Microbiol. 5 575–9
- [15] Kessin R H 2001 Dictyostelium: Evolution, Cell Biology, and the Development of Multicellularity (Cambridge: Cambridge University Press)
- [16] Bonner J T 2009 The Social Amoebae: The Biology of Cellular Slime Molds (Princeton, NJ: Princeton University Press)

- [17] Devreotes P N and Zigmond S H 1988 Chemotaxis in eukaryotic cells: a focus on leukocytes and Dictyostelium Annu. Rev. Cell. Biol. 4 649–86
- [18] Bonner J T 2015 Cellular Slime Molds (Princeton, NJ: Princeton University Press)
- [19] Meinhardt H 1999 Orientation of chemotactic cells and growth cones: models and mechanisms J. Cell Sci. 112 2867–74
- [20] Neilson M P, Mackenzie J A, Webb S D and Insall R H 2011 Modeling cell movement and chemotaxis using pseudopod-based feedback SIAM J. Sci. Comput. 33 1035–57
- [21] Neilson M P, Veltman D M, van Haastert P J M, Webb S D, Mackenzie J A and Insall R H 2011 Chemotaxis: a feedback-based computational model robustly predicts multiple aspects of real cell behaviour PLoS Biol. 9 e1000618
- [22] Hecht I, Skoge M L, Charest P G, Ben-Jacob E, Firtel R A, Loomis W F, Levine H and Rappel W-J 2011 Activated membrane patches guide chemotactic cell motility PLoS Comput. Biol. 7 e1002044
- [23] Tang Y and Othmer H G 1995 Excitation, oscillations and wave propagation in a G-protein-based model of signal transduction in Dictyostelium discoideum *Phil. Trans. R.* Soc. B 349 179–95
- [24] Dallon J C and Othmer H G 1997 A discrete cell model with adaptive signalling for aggregation of Dictyostelium discoideum *Phil. Trans. R. Soc.* B 352 391–417
- [25] Palsson E and Othmer H G 2000 A model for individual and collective cell movement in Dictyostelium discoideum *Proc. Natl Acad. Sci.* 97 10448–53
- [26] Dallon J C and Othmer H G 2004 How cellular movement determines the collective force generated by the Dictyostelium discoideum slug J. Theor. Biol. 231 203–22
- [27] Khamviwath V, Hu J and Othmer H G 2013 A continuum model of actin waves in Dictyostelium discoideum PLoS One 8 e64272
- [28] Cheng Y and Othmer H 2016 A model for direction sensing in Dictyostelium discoideum: ras activity and symmetry breaking driven by a $G_{\beta\gamma}$ -mediated, $G_{\alpha2}$ -Ric8—dependent signal transduction network *PLoS Comput. Biol.* 12 e1004900
- [29] Bretschneider T, Othmer H G and Weijer C J 2016 Progress and perspectives in signal transduction, actin dynamics, and movement at the cell and tissue level: lessons from Dictyostelium *Interface Focus* 6 20160047
- [30] Dallon J C and Othmer H G 1998 A continuum analysis of the chemotactic signal seen bydictyostelium discoideum J. Theor. Biol. 194 461–83
- [31] Wilhelm C, Riviere C and Biais N 2007 Magnetic control of Dictyostelium aggregation *Phys. Rev.* E 75 041906
- [32] Janmey P A and McCulloch C A 2007 Cell mechanics: integrating cell responses to mechanical stimuli *Annu. Rev. Biomed. Eng.* 9 1–34
- [33] Rivière C, Marion S, Guillén N, Bacri J-C, Gazeau F and Wilhelm C 2007 Signaling through the phosphatidylinositol 3-kinase regulates mechanotaxis induced by local low magnetic forces in Entamoeba histolytica J. Biomech. 40 64–77
- [34] Décavé E, Rieu D, Dalous J, Fache S, Bréchet Y, Fourcade B, Satre M and Bruckert F 2003 Shear flow-induced motility of Dictyostelium discoideum cells on solid substrate J. Cell Sci. 116 4331–43
- [35] Holmes W R and Edelstein-Keshet L 2012 A comparison of computational models for eukaryotic cell shape and motility PLoS Comput. Biol. 8 e1002793
- [36] Van Haastert P J M 2011 Amoeboid cells use protrusions for walking, gliding and swimming PloS One 6 e27532
- [37] Barry N P and Bretscher M S 2010 Dictyostelium amoebae and neutrophils can swim Proc. Natl Acad. Sci. 107 1376–80
- [38] Franz A, Wood W and Martin P 2018 Fat body cells are motile and actively migrate to wounds to drive repair and prevent infection *Dev. Cell* 44 460–70

- [39] Wang Q and Othmer H G 2016 Computational analysis of amoeboid swimming at low Reynolds number J. Math. Biol. 72 1893–926
- [40] Wu H, Thiébaud M, Hu W F, Farutin A, Rafaï S, Lai M C, Peyla P and Misbah C 2015 Amoeboid motion in confined geometry Phys. Rev. E 92 050701
- [41] Wu H, Farutin A, Hu W-F, Thiébaud M, Rafaï S, Peyla P, Lai M-C and Misbah C 2016 Amoeboid swimming in a channel Soft Matter 12 7470–84
- [42] Aoun L et al 2020 Amoeboid swimming is propelled by molecular paddling in lymphocytes Biophys. J. 119 1157–77
- [43] Dalal S, Farutin A and Misbah C 2020 Amoeboid swimming in a compliant channel *Soft Matter* 16 1599–613
- [44] Farutin A, Rafaï S, Dysthe D K, Duperray A, Peyla P and Misbah C 2013 Amoeboid swimming: a generic self-propulsion of cells in fluids by means of membrane deformations *Phys. Rev. Lett.* 111 228102
- [45] Bouffanais R and Yue D K 2010 Hydrodynamics of cell-cell mechanical signaling in the initial stages of aggregation Phys. Rev. E 81 041920
- [46] Campbell E J and Bagchi P 2017 A computational model of amoeboid cell swimming Phys. Fluids 29 101902
- [47] Campbell E J and Bagchi P 2020 A computational study of amoeboid motility in 3D: the role of extracellular matrix geometry, cell deformability, and cell–matrix adhesion Biomech. Model. Mechanobiol. 20 167–91
- [48] Shapere A and Wilczek F 1987 Self-propulsion at low Reynolds number Phys. Rev. Lett. 58 2051
- [49] Shapere A and Wilczek F 1989 Geometry of self-propulsion at low Reynolds number J. Fluid Mech. 198 557–85
- [50] Avron J E, Gat O and Kenneth O 2004 Optimal swimming at low Reynolds numbers Phys. Rev. Lett. 93 186001
- [51] Grossman N, Ron E Z and Woldringh C L 1982 Changes in cell dimensions during amino acid starvation of Escherichia coli J. Bacteriol. 152 35–41
- [52] Fu H C, Powers T R and Stocker R 2012 Bacterial rheotaxis Proc. Natl Acad. Sci. 109 4780-5
- [53] Pan M, Neilson M P, Grunfeld A M, Cruz P, Wen X, Insall R H and Jin T 2018 A G-protein-coupled chemoattractant receptor recognizes lipopolysaccharide for bacterial phagocytosis PLoS Biol. 16 e2005754
- [54] Cosson P and Soldati T 2008 Eat, kill or die: when amoeba meets bacteria Curr. Opin. Microbiol. 11 271–6
- [55] Bottino D C 2001 Computer simulations of mechanochemical coupling in a deforming domain: applications to cell motion *Mathematical Models for Biological Pattern Formation* (New York: Springer) pp. 295–314
- [56] Dillon R, Owen M and Painter K 2008 A single-cell-based model of multicellular growth using the immersed boundary method AMS Contemp. Math. 466 1–15
- [57] Börgers C and Peskin C S 1987 A Lagrangian fractional step method for the incompressible Navier–Stokes equations on a periodic domain *J. Comput. Phys.* 70 397–438 Börgers C and Peskin C S 1987 *J. Comput. Phys.* 466 1–5
- [58] Bae A J and Bodenschatz E 2010 On the swimming of Dictyostelium amoebae Proc. Natl Acad. Sci. 107 E165–6
- [59] Muskhelishvili N I 2013 Some Basic Problems of the Mathematical Theory of Elasticity (Berlin: Springer)
- [60] Cross M C and Hohenberg P C 1993 Pattern formation outside of equilibrium Rev. Mod. Phys. 65 851
- [61] Elliott C M, Stinner B and Venkataraman C 2012 Modelling cell motility and chemotaxis with evolving surface finite elements J. R. Soc. Interface 9 3027–44
- [62] Jana S, Um S H and Jung S 2012 Paramecium swimming in capillary tube Phys. Fluids 24 041901
- [63] Ledesma-Aguilar R and Yeomans J M 2013 Enhanced motility of a microswimmer in rigid and elastic confinement *Phys. Rev. Lett.* 111 138101
- [64] Sokolov A, Aranson I S, Kessler J O and Goldstein R E 2007 Concentration dependence of the collective dynamics of swimming bacteria Phys. Rev. Lett. 98 158102

[65] Lushi E, Goldstein R E and Shelley M J 2012 Collective chemotactic dynamics in the presence of self-generated fluid flows *Phys. Rev.* E 86 040902

- [66] Lushi E, Goldstein R E and Shelley M J 2018 Nonlinear concentration patterns and bands in autochemotactic suspensions *Phys. Rev.* E 98 052411
- [67] Nejad M R and Najafi A 2019 Chemotaxis mediated interactions can stabilize the hydrodynamic instabilities in active suspensions Soft Matter 15 3248–55
- [68] Partridge J D, Nhu N T Q, Dufour Y S and Harshey R M 2019 Escherichia coli remodels the chemotaxis pathway for swarming mBio 10 e00316-9
- [69] Ryan S D 2019 Role of hydrodynamic interactions in chemotaxis of bacterial populations *Phys. Biol.* 17 016003
- [70] Xue C, Hwang H J, Painter K J and Erban R 2011 Travelling waves in hyperbolic chemotaxis equations *Bull. Math. Biol.* 73 1695